

## Journal Pre-proofs

Anomalous Hall and Nernst Conductivities in  $rmCo_2$  NbGa: A first principles study

P. Rambabu, C.V. Anusree, M. Manivel Raja, V. Kanchana

PII: S0304-8853(21)00579-5

DOI: <https://doi.org/10.1016/j.jmmm.2021.168303>

Reference: MAGMA 168303

To appear in: *Journal of Magnetism and Magnetic Materials*

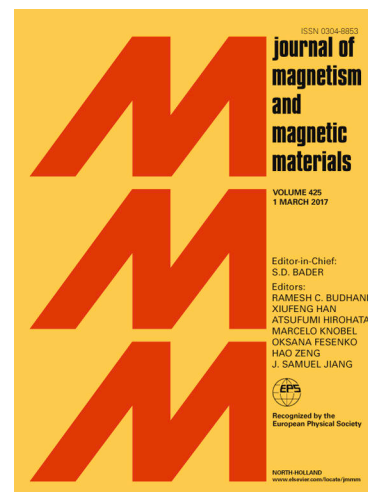
Received Date: 13 April 2021

Accepted Date: 13 July 2021

Please cite this article as: P. Rambabu, C.V. Anusree, M.M. Raja, V. Kanchana, Anomalous Hall and Nernst Conductivities in  $rmCo_2$  NbGa: A first principles study, *Journal of Magnetism and Magnetic Materials* (2021), doi: <https://doi.org/10.1016/j.jmmm.2021.168303>

This is a PDF file of an article that has undergone enhancements after acceptance, such as the addition of a cover page and metadata, and formatting for readability, but it is not yet the definitive version of record. This version will undergo additional copyediting, typesetting and review before it is published in its final form, but we are providing this version to give early visibility of the article. Please note that, during the production process, errors may be discovered which could affect the content, and all legal disclaimers that apply to the journal pertain.

© 2021 Published by Elsevier B.V.



# Anomalous Hall and Nernst Conductivities in Co<sub>2</sub>NbGa: A first principles study

P. Rambabu<sup>1,2</sup>, Anusree C. V.<sup>1</sup>, M. Manivel Raja<sup>3</sup>, V. Kanchana<sup>1,\*</sup>

<sup>1</sup>*Department of Physics, Indian Institute of Technology Hyderabad, Kandi - 502285, Sangareddy, Telangana, India.*

<sup>2</sup>*Department of Pure and Applied Physics, Guru Ghasidas Vishwavidyalaya, Koni, Bilaspur, 495009, Chattisgarh, India.*

<sup>3</sup>*Advanced Magnetic Group, Defence Metallurgical Research Laboratory, Kanchanbag P.O-500058, Hyderabad, Telangana, India.*

---

## Abstract

The ground state electronic, magnetic and elastic properties of Co<sub>2</sub>NbGa are studied using first-principles calculations. The investigated system is mechanically and dynamically stable which is confirmed through Born mechanical stability criteria and positive phonon modes. Two kinds of disorders B2 and D0<sub>3</sub>-types are studied to ensure the experimental magnetic moment in Co<sub>2</sub>NbGa within coherent potential approximation(CPA). The intrinsic anomalous Hall effect and anomalous Nernst effect are analysed from the Berry curvature point of view. The value of anomalous Hall conductivity and anomalous Nernst conductivity is 214.2 S/cm and -2.53 Am<sup>-1</sup>K<sup>-1</sup> within the range of  $\pm 300$ meV around Fermi level respectively, and the same are comparable with the values of other Heusler alloys. The Curie temperature ( $T_C$ ) is estimated up to 548.7 K through the Heisenberg magnetic exchange interactions within mean-field approximation. Half-metal to a metal transition under pressure is evidenced through band structure and Fermi surface topology. Also the magnetic, Heisenberg exchange, elastic properties are probed under pressure.

**Keywords:** Fermi surface, Berry Curvature, Anomalous Hall effect,

---

*Email address:* [kanchana@iith.ac.in](mailto:kanchana@iith.ac.in) (P. Rambabu<sup>1,2</sup>, Anusree C. V.<sup>1</sup>, M. Manivel Raja<sup>3</sup>, V. Kanchana<sup>1,\*</sup>)

## 1. Introduction

Heusler alloys have attracted researchers across the world not only due to their attractive properties but also due to their potential applications in several important areas such as spintronics[1, 2], spin-gapless semiconductors[3, 4], spin-gapless half metals[5], thermoelectricity[6, 7], topological insulators[8, 9], superconductors[10], shape memory alloys[11], etc. Especially, the full Heusler half-metallic alloys have captured much more attention because of their ability to have high degree of spin polarization[12, 13], high Curie temperature[14, 15], and lattice constant compatibility with semiconductors such as GaAs, InAs, InP, etc. making them highly suitable in the field of spintronics as potential candidates in spin injecting devices[16], spin filtering devices[17], magnetic tunnel junction (MTJ) devices[18, 19], and magneto-resistive devices[20]. In general, the ferromagnetic half metals are conducting in one spin channel, while in the other spin channel they are insulating/semiconducting. The ternary full Heusler alloys exist in  $X_2YZ$  cubic structure[21, 22]. Here X and Y are 3d, 4d or 5d transition metal elements and Z is the sp-element[21, 22] which is usually non-magnetic from group III, IV or V from the periodic table.

There are two types of Hall effects found in a solid in general, one is the ordinary Hall effect and the second one is the Anomalous Hall effect (AHE). The ordinary Hall effect is nothing but the generation of transverse voltage due to Lorentz force when a magnetic field is applied perpendicular to the applied current, which is observed in conventional metals or semiconductors[23]. In ferromagnetic or ferrimagnetic materials, a transverse voltage is developed additionally due to the spontaneous magnetization which causes the charge carriers to be deflected by magnetic moment with the strength of spin-orbit coupling is called the anomalous Hall effect. It does exist even in the absence of an applied magnetic field mainly due to the extrinsic mechanisms such as skew scattering[24], side jump[25], etc. and the intrinsic mechanisms such as Karplus-

Luttinger[26] and Berry curvature[27, 23, 28, 29, 30]. The intrinsic mechanism  
30 is connected to Berry curvature and there are numerous ways to understand the  
origin of AHE both experimentally and theoretically from the point of Berry  
curvature. Berry curvature is nothing but a band structure property of a solid  
material that provides the topological properties[31] of that material and the  
Berry curvature results because of entangled electronic Bloch bands with the  
35 inclusion of spin-orbit coupling, with time-reversal symmetry is broken due to  
spontaneous magnetization[32]. The AHE is reported in many ferromagnetic  
Heusler alloys[9]. The giant AHE is reported in magnetic Heusler compound  
 $\text{Co}_2\text{MnAl}$ [33]. Recently Shi et al.[34] reported large intrinsic anomalous Hall  
conductivity of about  $300 \text{ S/cm}$  for  $\text{Ti}_2\text{MnAl}$  and Markou et al.[35] reported a  
40 huge value of  $1138 \text{ S/cm}$  for  $\text{Co}_2\text{MnGa}$  compound. Recently, the authors[36]  
have synthesized  $\text{Co}_2\text{NbGa}$  cubic Heusler alloy experimentally for which there  
are no AHE studies available experimentally as well as theoretically. Motivated  
by these previous results, we expect the compound  $\text{Co}_2\text{NbGa}$  being the ferro-  
magnetic half metal to show up AHE, which we will discuss in the latter part  
45 of the paper.

The present paper is organized as follows: firstly the computational details  
of the various codes that are used for the calculations are discussed. Then  
the ground state electronic, magnetic, and disorder properties of the compound  
 $\text{Co}_2\text{NbGa}$  are discussed in the Results and discussions section. The anomalous  
50 Hall effect and Nernst effect of  $\text{Co}_2\text{NbGa}$  are also discussed here. The Heisenberg  
magnetic exchange interactions and hence Curie temperature are studied using  
mean-field approximation. The mechanical and phonon dispersion calculations  
are also discussed. Then, the half-metal to metallic transition is discussed under  
pressure for  $\text{Co}_2\text{NbGa}$  along with the variation of other physical properties with  
55 pressure. Finally, it is ended with conclusions and acknowledgments.

## 2. Computational details

All the electronic, magnetic, and elastic properties of  $\text{Co}_2\text{NbGa}$  are calculated within Density Functional Theory (DFT) as implemented in Vienna Ab-Initio Simulation Package (VASP)[37, 38]. The projector-augmented wave (PAW) method[39] is used to describe the electron-ion interactions. The expansion of Kohn-Sham states into plane-wave basis is done up to a kinetic energy cutoff of 516 eV. A Monkhorst-Pack[40] k-point grid of  $16 \times 16 \times 16$  is used for Brillouin zone sampling. The generalized-gradient approximation (GGA) by Perdew, Burke, and Ernzerhof[41] is used to describe the exchange and correlations in the system. The optimization is done up to a force convergence of  $10^{-2}$  eV/Å and the electronic convergence is achieved up to  $10^{-6}$  eV. The phonon band dispersion and phonon density of states are calculated using Density Functional Perturbation theory (DFPT) method as implemented in PHONOPY[42] package. For this, we used  $2 \times 2 \times 2$  supercell of primitive  $\text{Co}_2\text{NbGa}$  with 16 Co, 8 Nb, and 8 Ga atoms respectively and a k-mesh of  $2 \times 2 \times 2$  is used. For the Heisenberg magnetic exchange interactions and hence to estimate the mean-field Curie temperature ( $T_C$ ), we used the Green's function multiple scattering theory implemented in the spin-polarized relativistic Korringa-Kohn-Rostoker (SPR-KKR) package[43]. The full potential spin-polarized scalar relativistic Hamiltonian with  $l_{max}=3$  is used here and for Brillouin Zone integration a k-mesh of  $35 \times 35 \times 35$  is used. The disorder studies are carried out in SPRKKR using Coherent Potential Approximation (CPA)[44]. The anomalous Hall conductivity is calculated using wannier90[45] and wannier\_tools[46] packages with a k-point mesh of  $201 \times 201 \times 201$ .

## 3. Results and discussions

### 3.1. Ground State, Electronic and Magnetic Properties

The compound  $\text{Co}_2\text{NbGa}$  exists in cubic crystal structure with L21 phase as shown in Fig. 1. Fig. 1(a) and (b) show the conventional unit cell of  $\text{Co}_2\text{NbGa}$  in which a total of 16 atoms are present, while Fig. 1(c) shows the primitive

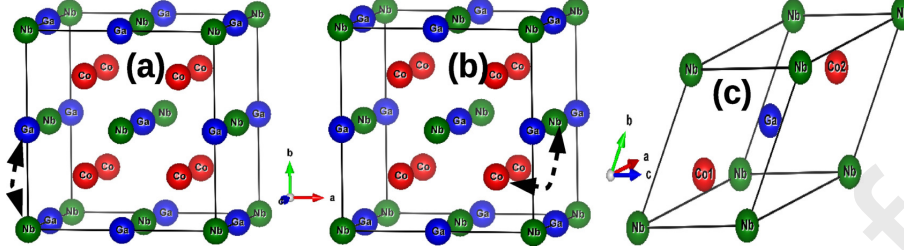


Figure 1: The cubic L21 crystal structure of Co<sub>2</sub>NbGa in Conventional cell with B2-type anti-site disorder (Nb atom goes into Ga and Ga atom goes into Nb simultaneously) in (a) and D0<sub>3</sub>-type anti-site disorder ((Co atom goes into Nb and Nb atom goes into Co simultaneously)) in (b). The Primitive unit cells with Co, Nb and Ga at (1/4, 1/4, 1/4), (0, 0, 0) and (1/2, 1/2, 1/2) respectively in (c).

85 cell of Co<sub>2</sub>NbGa which consists of only 4 atoms in it. Here the atoms Co, Nb and Ga occupy the (1/4, 1/4, 1/4), (0, 0, 0) and (1/2, 1/2, 1/2) positions respectively. The optimized lattice constant 5.97 Å is almost close to that of the experimental one 5.95 Å[36] which is shown in Table. 1. In general, Slater-Pauling[47] behavior is exhibited by half metals which is given by the rule

$$M_t = Z_t - 24 \quad (1)$$

90 for the L21 Heusler half metals, where  $M_t$  and  $Z_t$  are the total magnetic moment in  $\mu_B$  per f.u., and the total number of valence electrons respectively. The total magnetic moment of the compound is 2  $\mu_B$ /f.u. which follows the Slater-Pauling rule indicating that the studied compound is a half-metal. The obtained magnetic moment of Co is 1.03  $\mu_B$  and the induced moment on Nb is -0.03  $\mu_B$  which are shown in Table. 2.

The band structure of Co<sub>2</sub>NbGa is shown in Fig. 2(a). The solid black and dashed blue lines represent the majority and minority spin bands here. From Fig. 2(a), the compound is found to be insulating in minority spin case, while metallic in the majority spin case as there are band crossings found across Fermi level  $E_F$  along  $\Gamma - X$ ,  $\Gamma - K$  and  $\Gamma - W$  high symmetry directions. This clearly

100

Table 1: Experimental and optimized lattice constants in Å and Curie temperatures in K.

	a(expt)	a(opt)	$T_C$ (expt)	$T_C$ (MFA)
Co <sub>2</sub> NbGa	5.958[36]	5.97	351[36]	548.7

Table 2: Magnetic moment given in Bohr magneton ( $\mu_B$ ) for the individual atoms of Co<sub>2</sub>NbGa in ferromagnetic (FM) configuration.

	Co	Nb	Ga	Total/cell(theoretical)	Total/cell(expt)
Co <sub>2</sub> NbGa	1.028	-0.035	0.001	2.0001	1.81[36]

manifests the half-metallicity in this compound. The partial density of states of Co and Nb atoms in the majority and minority spin cases are shown in Fig. 2(b). From Fig. 2(b), it clear that the Co-d states are contributing significantly near  $E_F$  to the total DOS compared to Nd-d states. Next, we have calculated the Fermi surface for the spin-up channel which is shown in the supplementary sheet in Fig. S2. The hole characteristics with the open surface at high symmetry point X is shown by the band crossing the Fermi level along  $\Gamma - X$ . The Fermi surface corresponding to the band crossing the Fermi level twice along  $\Gamma - K$  from the valence band to conduction band and vice versa is showing a closed contour nature. This similar nature is observed along  $\Gamma - W$  also. A significant contribution of Co-d states is found near the Fermi level when compared to the other states. The crossing point near the Fermi level along  $\Gamma - X$  where mixed d-states of Co are present, opens up with the inclusion of spin-orbit coupling when the degeneracy is being lifted up. Depending upon the direction of magnetisation in combination with spin-orbit coupling the symmetry of the system is broken, which results in large Berry curvature being induced in the vicinity of Fermi energy. The non-vanishing valleys and peaks of the Berry curvature with the inclusion of spin-orbit coupling lead to the AHE. An important aspect

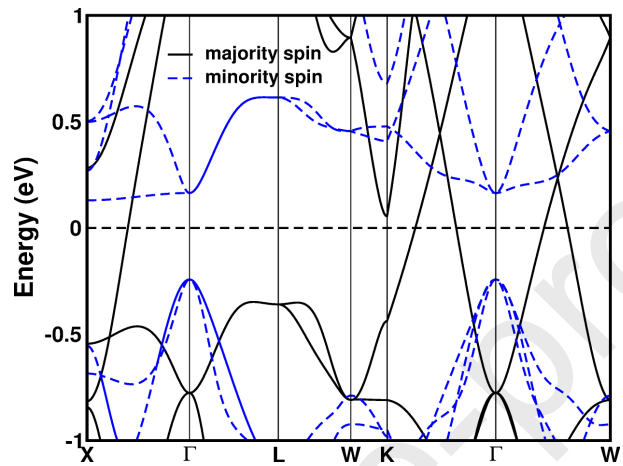
for a well defined net Berry curvature with a non-zero AHE comes from the  
 120 absence of symmetries, resulting in the reversal of the sign of local Berry curva-  
 ture in the Brillouin zone when the sign of momentum vector gets reversed eg:  
 time-reversal symmetries and mirror operations. Consequently, with suitable  
 manipulation of symmetries and band structures, Berry curvature and intrinsic  
 AHE can be restrained which is independent of the finite value of magnetiza-  
 125 tion. A similar kind of band structure can be seen in the Heusler series  $\text{Co}_2\text{TiX}$   
 ( $X=\text{Si, Ge or Sn}$ ) which is found to be topologically strong with Weyl fermion  
 as well as nodal line semimetal states [48]. These compounds were also found to  
 be potential candidates for applications of the anomalous Hall effect. A detailed  
 analysis is given in the latter section.

130 For spintronics applications, 100% spin polarization of material is desired.  
 The spin polarization of a ferromagnetic compound is determined from the  
 knowledge of the density of states of spin-up and spin-down at Fermi level  $E_F$ .  
 The percentage of spin polarization (P%) can be determined from the equation:

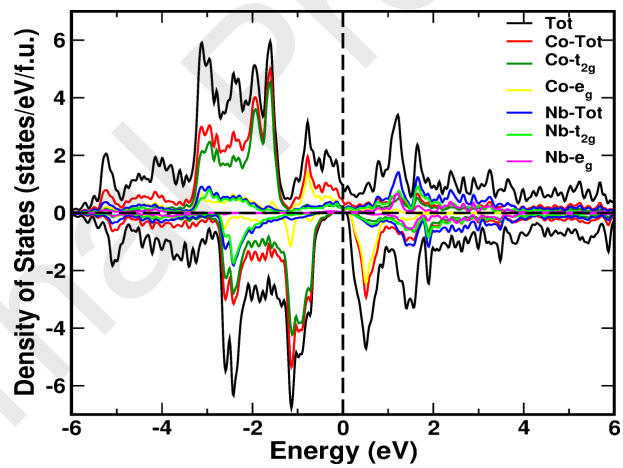
$$P\% = \frac{N \uparrow (E_F) - N \downarrow (E_F)}{N \uparrow (E_F) + N \downarrow (E_F)} \times 100 \quad (2)$$

where  $N \uparrow$  and  $N \downarrow$  are the density of states that contribute at Fermi level  $E_F$   
 135 in the majority and minority spin channels. The percentage of spin polarization  
 (P%) is found to be 100% for  $\text{Co}_2\text{NbGa}$  compound as there is no density of  
 states  $N \downarrow$  available at  $E_F$ . This implies that  $\text{Co}_2\text{NbGa}$  is useful in spintronics  
 applications.

The total magnetic moment obtained is  $2 \mu_B$ , but the experimental moment  
 140 is  $1.81 \mu_B$  and this discrepancy might be due to the presence of B2-type or  
 D0<sub>3</sub>-type disorders in the system. For B2-type, the anti-site disorder is realized  
 between Nb and Ga atoms, while for D0<sub>3</sub>-type the anti-site disorder is between  
 Co and Nb atoms. However, the mixing between two pairs of atoms is taken into  
 account simultaneously in both types of disorders which is shown in Fig. 1 (a)  
 145 and (b). Table. 3 shows the Co and total magnetic moments along with Curie  
 temperatures for different degrees of disorder for B2 and D0<sub>3</sub>-type cases. From



(a)



(b)

Figure 2: The majority and minority spin band structure of  $\text{Co}_2\text{NbGa}$  in (a) The partial density of states of Co and Nb atoms are shown in (b).

Table. 3, it clear that for B2-type 50% disorder, the total magnetic moment is coming out to be  $1.88 \mu_B$  which is close to the experimental moment  $1.81 \mu_B$ . From this, one may conclude that B2-type disorder may be present in the experimentally synthesized compound.

Table 3: B2 and D0<sub>3</sub> with different types of anti-site disorder for various degrees. Magnetic moments are given in Bohr magneton ( $\mu_B$ ) and the Curie temperature  $T_C$  is given in the units of *Kelvin*.

Type	Degree of Disorder	Co-moment	Total Moment/f.u.	$T_C$
B2	0.0%	1.0203	1.9962	548.7
—	10%	0.9845	1.9828	411.0
—	20%	0.9546	1.9434	326.1
—	30%	0.9327	1.9099	274.0
—	40%	0.9190	1.8878	245.2
—	50%	0.9146	1.8800	236.3
D0 <sub>3</sub>	0.0%	1.0203	1.9962	548.7
—	10%	0.9419	1.9251	399.4
—	20%	0.7292	1.2466	200.9
—	30%	0.8747	2.0055	261.7
—	40%	0.8932	2.1224	257.1
—	50%	0.9481	2.2733	268.0

### 3.2. Anomalous Hall and Nernst effect

From the obtained tight binding Hamiltonian using wannier90 code, the Berry curvature  $\Omega_B(k)$  or  $\Omega_{n,ij}(k)$ [30] can be expressed as:

$$\Omega_{n,ij}(k) = \sum_{n \neq m} \frac{\langle n | \frac{\partial H}{\partial K_i} | m \rangle \langle m | \frac{\partial H}{\partial K_j} | n \rangle - (i \leftrightarrow j)}{(\epsilon_n - \epsilon_m)^2} \quad (3)$$

where n and m are the eigenstates and  $\epsilon_n$  and  $\epsilon_m$  are their corresponding eigen-energies of the Hamiltonian H. Then the Anomalous Hall conductivity  $\sigma_{xy}^A$ [49]

derived from Berry curvature  $\overline{\Omega_B(k)}$  can be written as:

$$\sigma_{xy}^A = \frac{-e^2}{\hbar} \int_{BZ} \frac{d^3k}{(2\pi)^3} f(k) \Omega_B(k) \quad (4)$$

where  $f(k)$  is the Fermi-Dirac distribution function,  $e$  is the charge on electron and  $\hbar$  is the reduced Planck's constant. The Anomalous Nernst effect (ANE)[50, 51] is defined as the generation of transverse electric voltage in a magnetic material that is perpendicular to both magnetization and an applied thermal gradient. It is known as the thermoelectric counterpart of the AHE[52]. Berry curvature or the nontrivial geometric structure of the wavefunction of electrons[50] drives the ANE which is also proportional to magnetization[51]. Now, the anomalous off-diagonal thermoelectric coefficient which is nothing but the Anomalous Nernst Conductivity (ANC)  $\alpha_{xy}^A$ [49] can be expressed as:

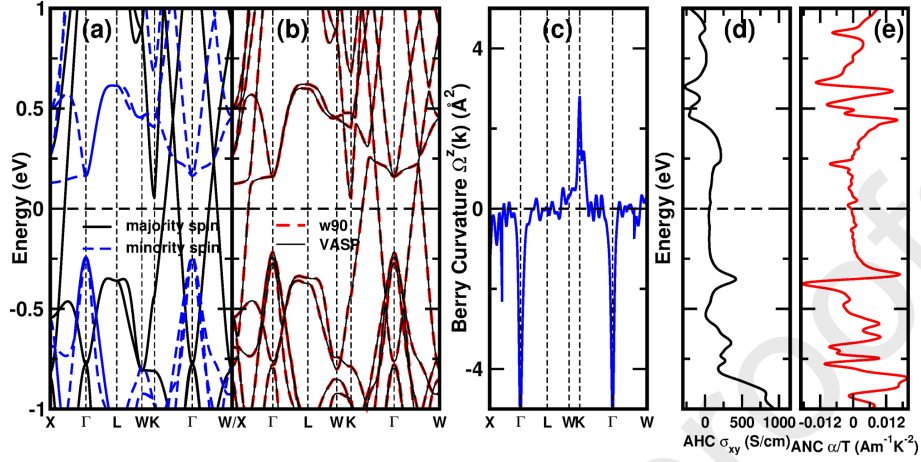
$$\alpha_{xy}^A(T, \mu) = -\frac{1}{e} \int_{BZ} d\epsilon \frac{\partial f(\epsilon - \mu, T)}{\partial \epsilon} \cdot \frac{\epsilon - \mu}{T} \sigma_{xy}^A(\epsilon) \quad (5)$$

where  $\mu$  is the chemical potential. Near zero temperature, the above equation[49] becomes,

$$\left. \frac{\alpha_{xy}^A}{T} \right|_{T \rightarrow 0} = -\frac{\pi^2}{3} \frac{k_B^2}{|e|} \frac{d\sigma_{xy}^A}{d\mu} \quad (6)$$

where  $k_B$  is Boltzmann's constant.

The high symmetry path-dependent Berry curvature  $\Omega^z(k)$  of  $\text{Co}_2\text{NbGa}$  is shown in Fig. 3(c) and the band structure of  $\text{Co}_2\text{NbGa}$  without and with spin-orbit coupling (SOC) along with AHC and ANC within the energy range of -1.0-1.0 eV is shown in Fig. 3(a,b and d). From Fig. 3(c), it is clear that the Berry curvature is non-vanishing and is having peaks above and below Fermi level  $E_F$  along different paths. The non-vanishing valleys and peaks of the Berry curvature is due to the pair of spin-orbit coupled bands[53]. Due to the application of spin-orbit coupling, the small opening of the energy gap gives the small denominator in the equation. 3, which causes the large Berry curvature. From Fig. 3(b), it is seen that the DFT band structure with SOC is very well matched with the wannier90 interpolated band structure. The AHC is shown in Fig. 3(d) as a function of  $E - E_F$  (eV) and we have considered  $\pm 300\text{meV}$



(a)

Figure 3: The band structure of  $\text{Co}_2\text{NbGa}$  (a) without SOC, (b) with the inclusion of spin-orbit coupling (the band structures using VASP and wannier90 are shown in dashed red and solid black lines respectively), (c) Berry curvature  $\Omega^z(k)$  of  $\text{Co}_2\text{NbGa}$  along high symmetry path, (d) The Anomalous Hall Conductivity  $\sigma_{xy}$  and (e) The Anomalous Nernst Conductivity  $\alpha/T$  of  $\text{Co}_2\text{NbGa}$ . The calculated values of  $\sigma_{xy}$  and  $\alpha$  at  $300\text{K}$  respectively are  $214.2\text{ S/cm}$  and  $-2.53\text{ Am}^{-1}\text{K}^{-1}$  at  $223.2\text{ eV}$  within the range of  $\pm 300\text{meV}$  around Fermi level  $E_F$ .

165 range from Fermi level  $E_F$  to find out the maximum value of AHC. Within this range, the maximum AHC is found to be  $214.2\text{ S/cm}$  around  $+266\text{ meV}$  which is comparable to the AHC values of other Heusler compounds[9]  $\text{Co}_2\text{TiAl}$  ( $-244\text{ S/cm}$ ),  $\text{Co}_2\text{TiGe}$  ( $-297\text{ S/cm}$ ) and  $\text{Co}_2\text{TiGe}$  ( $-285\text{ S/cm}$ ) etc. The ANC  $\frac{\alpha}{T}$  ( $\text{Am}^{-1}\text{K}^{-2}$ ) as a function of  $E - E_F$  (eV) is plotted in Fig. 3(d). From  
 170 equation 6, the maximum ANC value within  $\pm 300\text{meV}$  range is found to be  $-2.53\text{ Am}^{-1}\text{K}^{-1}$  at  $223.2\text{ meV}$  at room temperature.

### 3.3. Magnetic Exchange interactions

The magnetic interactions in Co<sub>2</sub>NbGa are probed via Heisenberg exchange coupling  $J_{ij}$ . The positive and negative values of  $J_{ij}$  respectively indicate the  
 175 ferromagnetic (FM) and anti-ferromagnetic (AFM) couplings between atoms. Using the classical Heisenberg exchange Hamiltonian that describes the magnetic exchange coupling  $J_{ij}$  between atoms as given by [54, 55]

$$H_{eff} = - \sum_{\mu\nu} \sum_{ij} J_{ij}^{\mu\nu} e_i^\mu e_j^\nu \quad (7)$$

where  $\mu$  and  $\nu$  are specific sublattices,  $i$  and  $j$  indicate atomic positions respectively, and  $e_i^\mu$ ,  $e_j^\nu$  indicate the magnetic moment's direction of  $i$ ,  $j$  atoms in  
 180 sublattices  $\mu$  and  $\nu$  respectively. The Curie temperature ( $T_C$ ) is expressed as

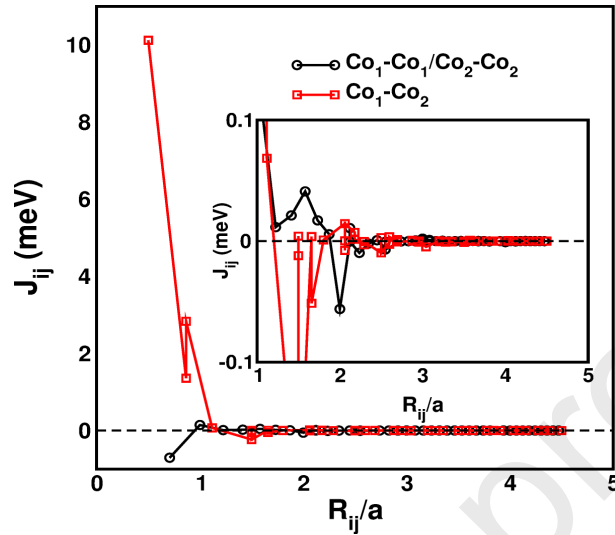
$$T_C = \frac{2}{3k_B} J_{max} \quad (8)$$

Here  $J_{max}$  is the largest eigenvalue of the effective exchange coupling constant  $J_{eff}$  which is given by

$$J_{eff}^{\mu\nu} = \sum_{j \neq 0} J_{0j}^{\mu\nu} \quad (9)$$

where 0 represents a particular atomic position within the  $\mu$ -sublattice and  $j$  takes all atomic positions in the sublattice  $\nu$  in the sphere of radius  $4.5a$ , where  
 185  $a$  is the optimized equilibrium lattice constant of Co<sub>2</sub>NbGa.

The Heisenberg exchange coupling constant  $J_{ij}$  between the sites  $i$  and  $j$  is plotted as a function of  $R_{ij}/a$  in Fig. 4, where  $R_{ij}$  is the nearest neighbor distance and 'a' is the lattice parameter of the compound. Here the dominating contribution to exchange coupling  $J_{ij}$  mainly comes from Co<sub>1</sub>-Co<sub>2</sub> and Co<sub>1</sub>-  
 190 Co<sub>1</sub>/Co<sub>2</sub>-Co<sub>2</sub> interactions and the other interactions are not shown here as their contribution is almost negligible. For Co<sub>1</sub>-Co<sub>2</sub>, the first four nearest-neighbor interactions are positive and the fifth, sixth nearest-neighbor interactions are negative indicating RKKY-type interactions in this compound. But the FM nature of the interaction is retained in Co<sub>1</sub>-Co<sub>2</sub> interaction as the positive  $J_{ij}$



(a)

Figure 4: The Heisenberg exchange interactions for  $\text{Co}_2\text{NbGa}$ . The interactions between Co-Nb, Co-Ga, Nb-Nb, Nb-Ga and Ga-Ga are excluded in the plot as their contribution is almost negligible.

195 strength is more compared to that of the negative one. For  $\text{Co}_1\text{-Co}_1/\text{Co}_2\text{-Co}_2$  interaction, the first, second and the third nearest-neighbor interactions are negative, positive and negative respectively as shown in Fig. 4 which shows the oscillatory behavior indicating RKKY-type interaction. Though for both cases, the oscillatory behavior is observed, ultimately the positive interaction  
 200 dominates over negative interaction and the system remains to be ferromagnetic in nature. The Curie temperature ( $T_C$ ) of  $\text{Co}_2\text{NbGa}$  of estimated from mean-field approximation is  $548.7\text{ K}$  which is higher than that of experimental  $T_C$  value  $351\text{ K}$ . A similar trend was found for other Heusler compounds such as  $\text{Co}_2\text{CrAl}$  and  $\text{Co}_2\text{CrGe}$ [13].

### 205 3.4. Mechanical and Dynamical Stability

To ensure the phase stability of  $\text{Co}_2\text{NbGa}$  compound mechanically, we have computed elastic constants  $C_{ij}$  for the same compound. The values of three

elastic constants  $C_{11}$ ,  $C_{12}$  and  $C_{44}$  of cubic  $\text{Co}_2\text{NbGa}$  are tabulated in Table. 3.4. The calculated elastic constants of  $\text{Co}_2\text{NbGa}$  satisfy the Born mechanical stability criteria[56] i.e.  $C_{11} > 0$ ,  $C_{44} > 0$ ,  $C_{11} > C_{12}$  and  $C_{11} + 2C_{12} > 0$  ensuring the mechanical stability of the studied compound. In addition, the elastic properties are also computed and are also tabulated in Table. 3.4 which includes Young's modulus (E), average shear modulus (G), anisotropy factor (A), and Poisson's ratio, etc., and are derived from Voigt-Reuss-Hill approximation[57].

The relation among the other parameters and the elastic moduli  $C_{ij}$  are found elsewhere[58, 59, 60]. In general, the bulk modulus (B) is nothing but the compressibility of solids under hydrostatic pressure, the larger is B, the solid is more difficult to be compressed. The bulk modulus (B) for  $\text{Co}_2\text{NbGa}$  is 196.2 GPa indicating that it is hard to be compressed. The larger shear modulus (G) gives higher hardness and for  $\text{Co}_2\text{NbGa}$ , the G value is 81.7 GPa. Similarly, the stiffness of the material is related to Young's modulus (E), and the value of E for  $\text{Co}_2\text{NbGa}$  is 215.3 GPa is larger indicating the higher stiffness in the studied compound. The Poisson's ratio ( $\sigma$ ), Pugh's ratio (G/B), and Cauchy's pressure ( $P_C$ ) will give information about the ductility and brittleness of the solids. The solid is ductile if  $\sigma > 0.26$ ,  $C_{12} - C_{44} > 0$  and  $G/B < 0.57$ . Here the compound satisfies all three cases indicating  $\text{Co}_2\text{NbGa}$  to be ductile. For exploring microcracks in materials, the Anisotropy factor (A) is useful and the compound is anisotropic since A is different from unity. The Debye temperature ( $\Theta_D$ ) is one of the fundamental thermodynamic parameters of solids that distinguishes between high and low temperature regions of a solid, and can be calculated from the mean sound velocity as given in Table. 3.4. The value of Debye temperature ( $\Theta_D$ ) for  $\text{Co}_2\text{NbGa}$  is found to be 429.9 K.

The dynamical stability of  $\text{Co}_2\text{NbGa}$  is verified through phonon dispersion calculations and the dispersion plot along with phonon density of states is shown in Fig. 5. The positive values of phonon frequencies (absence of imaginary frequencies) are a clear indication of dynamical stability in the studied compound.

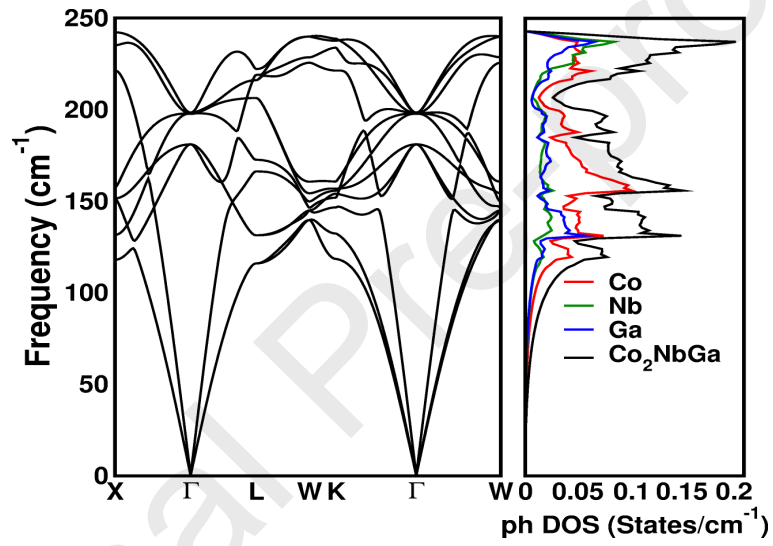


Figure 5: The phonon band dispersion along with phonon dispersion states of  $\text{Co}_2\text{NbGa}$  compound.

Table 4: Single crystalline elastic constants of  $\text{Co}_2\text{NbGa}$  at ambient pressure in GPa,  $E$  is Young's modulus in GPa,  $\sigma$  is Poisson's ratio,  $A$  is Anisotropy factor,  $P_C$ = Cauchy's pressure ( $C_{12}$ - $C_{44}$ ) in GPa,  $G/B$ = Pugh's ratio,  $V_l$ ,  $V_t$  nad  $V_m$  are longitudinal, transverse and mean sound velocities in  $km/sec$  and  $\Theta_D$  is Debye temperature in *Kelvin*.

Parameters	Value
$C_{11}$	266.4
$C_{12}$	161.2
$C_{44}$	109.8
Anisotropy factor $A$	2.08
$G_V$	86.91
$G_R$	76.51
$B$	196.2
$G$	81.7
$E$	215.3
$B/G$	2.40
Poisson's ratio $\sigma$	0.317
$P_C$	51.4
$G/B$	0.416
$V_l$	5.90
$V_t$	3.05
$V_m$	3.42
$\Theta_D$	429.9

### 3.5. Under Pressure

The pressure variation of different properties of  $\text{Co}_2\text{NbGa}$  is also studied. The mechanical stability of  $\text{Co}_2\text{NbGa}$  for 5, 10, and 15 GPa pressures is ensured via Born stability criteria. The phonon dispersion of  $\text{Co}_2\text{NbGa}$  for 5, 10 and 15 GPa pressures are given in Fig. S1(a,b,c). From the plots, it can be seen that the profile of phonon dispersion is similar to ambient calculations and no imaginary phonon modes are indicating that the compound is also found to be stable under the studied pressures. The frequency of phonon modes is found to be increased with pressure.

The band structure of  $\text{Co}_2\text{NbGa}$  without SOC for 0, 5, 10, and 15 GPa pressures are shown in supplementary sheet in Fig. S2 for both majority and minority spin cases with corresponding Fermi surface topology in Fig. S3. From Fig. S2(a) at 0 GPa, only two bands found to cross Fermi level  $E_F$  and their corresponding two Fermi surfaces are shown in Fig. S3 in the majority spin case. For 5 GPa pressure, there is no significant change in band structure as seen from Fig. S2(b). But when 10 GPa pressure is applied, apart from two crossing bands in majority spin case, another band found to cross  $E_F$  along  $\Gamma - X$  high symmetry direction in minority spin case as shown in Fig. S2(c) indicating a half-metallic to metallic transition in this compound. The transition is reflected in Fermi surface topology of  $\text{Co}_2\text{NbGa}$  in 10 GPa case as shown from Fig. S3 where an additional Fermi surface is found along  $\Gamma - X$  direction. Unfortunately, the compound  $\text{Co}_2\text{NbGa}$  loses its half-metallicity under an applied pressure of 10 GPa as both the majority and minority spin channels become conducting and the compound becomes a ferromagnetic metal. For 15 GPa, the band crosses  $E_F$  twice in minority spin case along  $\Gamma - X$  and around  $\Gamma$  two-band crossings are seen in the majority spin case as shown in Fig. S2(d) The Fermi surfaces for minority case at 15 GPa are shown in Fig. S3 which displays the two-electron pockets.

The variation of Co magnetic moment of  $\text{Co}_2\text{NbGa}$  is shown in Fig. S4(a) and Co moment is found to decrease from 1.02 to  $0.97 \mu_B$  up to studied pressure. The variation of the total magnetic moment of  $\text{Co}_2\text{NbGa}$  compound under

pressure is shown in Fig. S4(b) and the total moment is also found to decrease from 2.00 to 1.98  $\mu_B$  with pressure as Co moment decreases.

270 The variation of AHC and ANC of Co<sub>2</sub>NbGa for different pressures as a function of Energy (eV) is shown in Fig. S5 and their corresponding maximum values within the range of  $\pm 300 meV$  around Fermi level  $E_F$  are tabulated in Table. S1. From Table. S1, it is clear that the maximum value of AHC increases from 0 GPa to 15 GPa, whereas the maximum value of ANC at 300 K decreases  
275 systematically as we move from 0 GPa to 15 GPa.

The exchange coupling  $J_{ij}$  for different pressures is shown in Fig. S6. The first nearest-neighbor interactions for Co<sub>1</sub>-Co<sub>2</sub> for 0, 5, and 10 GPa pressures respectively are 10.12, 10.27, and 10.38  $meV$  and hence their Curie temperatures increase systematically as shown in Fig.S7(a). For 15 GPa pressure, the Curie  
280 temperature is found to decrease because of the more negative nature of the second nearest-neighbor interactions for Co<sub>1</sub>-Co<sub>1</sub>/Co<sub>2</sub>-Co<sub>2</sub> as shown in Fig. S6(d) which reduces the Curie temperature that can be seen from Fig.S7(a). The degree of spin polarization is found to decrease with applied pressure as shown in Fig. S7(b) and it is around 2.7% for 15 GPa which is due to the destruction  
285 of half-metallicity at 15 GPa. From this, we can say that Co<sub>2</sub>NbGa is not suitable for spintronics applications under pressure as it loses its half-metallicity completely under pressure.

The Elastic constants of Co<sub>2</sub>NbGa vs pressure plot are shown in Fig. S8(a). All the three  $C_{11}$ ,  $C_{12}$ ,  $C_{44}$  and the shear  $C_s = \frac{C_{11} - C_{12}}{2}$  are found to increase with  
290 pressure. Here,  $C_{11}$  is more sensitive to pressure while  $C_{44}$  is most insensitive to the applied pressure. The variation of all three elastic moduli  $B$ ,  $G$  and  $E$  with pressure is shown in Fig. S8(b). From Fig. S8(b), it is clear that all three moduli are found to increase linearly with an increase in pressure. Here Young's modulus  $E$  is most sensitive to pressure while the shear modulus  
295  $G$  is most insensitive. Under pressure, Young's modulus  $E$  increases rapidly indicating that Co<sub>2</sub>NbGa becomes more stiffer up to the pressure studied .

#### 4. Conclusion

In summary, the  $\text{Co}_2\text{NbGa}$  is found to be a half-metal that follows Slater-Pauling rule. From the two kinds of disorders studied B2 and  $\text{D0}_3$ , we conclude that nearly 50% B2-type disorder is present in the system. The Berry curvature derived anomalous Hall conductivity of  $\text{Co}_2\text{NbGa}$  is found to be  $214.2 \text{ S/cm}$  within the range of  $\pm 300 \text{ meV}$  around Fermi level  $E_F$  which is comparable to the values of other magnetic Heusler alloys. The anomalous Nernst conductivity within the same range around  $E_F$  is found to be  $-2.53 \text{ Am}^{-1}\text{K}^{-1}$  at room temperature. The Heisenberg exchange interactions among various atoms in  $\text{Co}_2\text{NbGa}$  are studied and hence Curie temperature is estimated from mean-field approximation which is coming out to be  $548.7 \text{ K}$ . The mechanical and dynamical stabilities of  $\text{Co}_2\text{NbGa}$  are ensured via Born stability criteria and phonon dispersion. Under pressure, the half-metallic  $\text{Co}_2\text{NbGa}$  turns out to be metallic which is evidenced through band structure and Fermi surface topology around 10 GPa. Also the variation of magnetic moments, Heisenberg exchange interactions  $J_{ij}$  and hence Curie temperature  $T_C$  and elastic constants as a function of pressure is studied.

#### 5. Acknowledgement

The authors PR and VK would like to thank IIT Hyderabad and National PARAM Supercomputing Facility (NPSF) and Centre for Development of Advanced Computing (C-DAC), Pune for computational facility and PR acknowledges Guru Ghasidas Vishwavidyalaya, Bilaspur, C.G. for sponsoring Ph.D. Anusree C.V and VK acknowledges DRDO project with reference number (ERIP/ER/201701001/M/01/-1711).

#### References

- [1] J. K. Kawasaki, APL Materials 7 (2019) 080907. doi:10.1063/1.5099576.

- [2] C. Guillemard, S. Petit-Watelot, J.-C. Rojas-Sánchez, J. Hohlfeld, J. Ghanbaja, A. Bataille, P. Le Fèvre, F. Bertran, S. Andrieu, *Appl. Phys. Lett.* 115 (2019) 172401. doi:10.1063/1.5121614.
- [3] Q. Gao, I. Opahle, H. Zhang, *Phys. Rev. Materials* 3 (2019) 024410. doi:10.1103/PhysRevMaterials.3.024410.
- [4] Z. Yue, Z. Li, L. Sang, X. Wang, *Small* 16 (2020) 1905155. doi:https://doi.org/10.1002/smll.201905155.
- [5] G. Y. Gao, K.-L. Yao, *Applied Physics Letters* 103 (2013) 232409. doi:10.1063/1.4840318.
- [6] Y. Shimanuki, K. Kudo, T. Ishibe, A. Masago, S. Yamada, Y. Nakamura, K. Hamaya, *J. of Appl. Phys.* 127 (2020) 055106. doi:10.1063/1.5141949.
- [7] S. A. Khandy, J.-D. Chai, *J. of Appl. Phys.* 127 (2020) 165102. doi:10.1063/1.5139072.
- [8] C. Mondal, C. K. Barman, B. Pathak, A. Alam, *Phys. Rev. B* 100 (2019) 245151. doi:10.1103/PhysRevB.100.245151.
- [9] J. Noky, Y. Zhang, J. Gooth, C. Felser, Y. Sun, *npj Computational Materials* 6 (2020) 1–8. doi:https://doi.org/10.1038/s41524-020-0342-5.
- [10] K. Górnicka, G. Kuderowicz, E. M. Carnicom, K. Kutorasiński, B. Wiendlocha, R. J. Cava, T. Klimczuk, *Phys. Rev. B* 102 (2020) 024507. doi:10.1103/PhysRevB.102.024507.
- [11] Y. Shen, Z. Wei, W. Sun, Y. Zhang, E. Liu, J. Liu, *Acta Materialia* 188 (2020) 677. doi:https://doi.org/10.1016/j.actamat.2020.02.045.
- [12] X. Hu, Y. Zhang, S. Fan, X. Li, Z. Zhao, C. He, Y. Zhao, Y. Liu, W. Xie, *Journal of Physics: Condensed Matter* 32 (2020) 205901. doi:10.1088/1361-648x/ab6e96.

- [13] P. Rambabu, B. Anuroopa, M. Manivel Raja, V. Kanchana, *Solid State Sciences* 105 (2020) 106257. doi:<https://doi.org/10.1016/j.solidstatesciences.2020.106257>.  
350
- [14] R. P. Dulal, B. R. Dahal, A. Forbes, I. L. Pegg, J. Philip, *Journal of Magnetism and Magnetic Materials* 423 (2017) 314. doi:<https://doi.org/10.1016/j.jmmm.2016.09.130>.
- [15] P. Midhunlal, J. A. Chelvane, U. A. Krishnan, D. Prabhu, R. Gopalan, N. H. Kumar, *Journal of Physics D: Applied Physics* 51 (2018) 075002. doi:<https://doi.org/10.1088/1361-6463/aaa564>.  
355
- [16] K. A. Kilian, R. H. Victora, *Journal of Applied Physics* 87 (2000) 7064–7066. doi:10.1063/1.372932.
- [17] J. Han, G. Gao, *Appl. Phys. Lett.* 113 (2018) 102402. doi:10.1063/1.5047151.  
360
- [18] Y. Sakuraba, J. Nakata, M. Oogane, H. Kubota, Y. Ando, A. Sakuma, T. Miyazaki, *Japanese Journal of Applied Physics* 44 (2005) L1100–L1102. doi:10.1143/jjap.44.11100.
- [19] Y. Sakuraba, M. Hattori, M. Oogane, Y. Ando, H. Kato, A. Sakuma, T. Miyazaki, H. Kubota, *Applied Physics Letters* 88 (2006) 192508. doi:10.1063/1.2202724.  
365
- [20] T. Iwase, Y. Sakuraba, S. Bosu, K. Saito, S. Mitani, K. Takanashi, *Applied Physics Express* 2 (2009) 063003. doi:10.1143/apex.2.063003.
- [21] T. Graf, F. Casper, J. Winterlik, B. Balke, G. H. Fecher, C. Felser, *Zeitschrift für anorganische und allgemeine Chemie* 635 (2009) 976–981.  
370
- [22] T. Graf, C. Felser, S. S. Parkin, *Progress in Solid State Chemistry* 39 (2011) 1–50. doi:<https://doi.org/10.1016/j.progsolidstchem.2011.02.001>.

- [23] H. Kontani, T. Tanaka, K. Yamada, Phys. Rev. B 75 (2007) 184416. doi:  
375 10.1103/PhysRevB.75.184416.
- [24] J. Smit, Physica 21 (1955) 877–887. doi:https://doi.org/10.1016/  
S0031-8914(55)92596-9.
- [25] L. Berger, Phys. Rev. B 2 (1970) 4559–4566. doi:10.1103/PhysRevB.2.  
4559.
- [26] R. Karplus, J. M. Luttinger, Phys. Rev. 95 (1954) 1154–1160. doi:10.  
380 1103/PhysRev.95.1154.
- [27] Y. Yao, L. Kleinman, A. H. MacDonald, J. Sinova, T. Jungwirth, D.-s.  
Wang, E. Wang, Q. Niu, Phys. Rev. Lett. 92 (2004) 037204. doi:10.  
1103/PhysRevLett.92.037204.
- [28] N. Nagaosa, J. Sinova, S. Onoda, A. H. MacDonald, N. P. Ong, Rev. Mod.  
385 Phys. 82 (2010) 1539–1592. doi:10.1103/RevModPhys.82.1539.
- [29] J. Kübler, C. Felser, Phys. Rev. B 85 (2012) 012405. doi:10.1103/  
PhysRevB.85.012405.
- [30] D. Xiao, M.-C. Chang, Q. Niu, Rev. Mod. Phys. 82 (2010) 1959–2007.  
390 doi:10.1103/RevModPhys.82.1959.
- [31] K. Manna, L. Muechler, T.-H. Kao, R. Stinshoff, Y. Zhang, J. Gooth,  
N. Kumar, G. Kreiner, K. Koepernik, R. Car, J. Kübler, G. H. Fecher,  
C. Shekhar, Y. Sun, C. Felser, Phys. Rev. X 8 (2018) 041045. doi:10.  
1103/PhysRevX.8.041045.
- [32] B. K. Hazra, S. N. Kaul, S. Srinath, M. M. Raja, R. Rawat, A. Lakhani,  
395 Phys. Rev. B 96 (2017) 184434. doi:10.1103/PhysRevB.96.184434.
- [33] Y. J. Chen, D. Basiaga, J. R. O’Brien, D. Heiman, Applied Physics Letters  
84 (2004) 4301–4303. doi:10.1063/1.1755842.

- [34] W. Shi, L. Muechler, K. Manna, Y. Zhang, K. Koepf, R. Car, J. van den  
400 Brink, C. Felser, Y. Sun, Phys. Rev. B 97 (2018) 060406. doi:10.1103/  
PhysRevB.97.060406.
- [35] A. Markou, D. Kriegner, J. Gayles, L. Zhang, Y.-C. Chen, B. Ernst, Y.-H.  
Lai, W. Schnelle, Y.-H. Chu, Y. Sun, C. Felser, Phys. Rev. B 100 (2019)  
054422. doi:10.1103/PhysRevB.100.054422.
- 405 [36] T. Kanomata, H. Nishihara, T. Osaki, M. Doi, T. Sakon, Y. Adachi, T. Ki-  
hara, K. Obara, T. Shishido, Journal of Magnetism and Magnetic Mate-  
rials 503 (2020) 166604. doi:https://doi.org/10.1016/j.jmmm.2020.  
166604.
- [37] G. Kresse, J. Furthmüller, Phys. Rev. B 54 (1996) 11169–11186. doi:  
410 10.1103/PhysRevB.54.11169.
- [38] G. Kresse, D. Joubert, Phys. Rev. B 59 (1999) 1758–1775. doi:10.1103/  
PhysRevB.59.1758.
- [39] P. E. Blöchl, Phys. Rev. B 50 (1994) 17953–17979. doi:10.1103/  
PhysRevB.50.17953.
- 415 [40] H. J. Monkhorst, J. D. Pack, Phys. Rev. B 13 (1976) 5188–5192. doi:  
10.1103/PhysRevB.13.5188.
- [41] J. P. Perdew, K. Burke, M. Ernzerhof, Phys. Rev. Lett. 77 (1996) 3865–  
3868. doi:10.1103/PhysRevLett.77.3865.
- [42] A. Togo, I. Tanaka, Scripta Materialia 108 (2015) 1–5. doi:https://doi.  
420 org/10.1016/j.scriptamat.2015.07.021.
- [43] H. Ebert, D. Ködderitzsch, J. Minár, Reports on Progress in Physics 74  
(2011) 096501. doi:10.1088/0034-4885/74/9/096501.
- [44] P. Soven, Phys. Rev. 156 (1967) 809–813. doi:10.1103/PhysRev.156.809.

- [45] G. Pizzi, V. Vitale, R. Arita, S. Blügel, F. Freimuth, G. Géranton, M. Gibertini, D. Gresch, C. Johnson, T. Koretsune, J. Ibañez-Azpiroz, H. Lee, J.-M. Lihm, D. Marchand, A. Marrazzo, Y. Mokrousov, J. I. Mustafa, Y. No-hara, Y. Nomura, L. Paulatto, S. Poncé, T. Ponweiser, J. Qiao, F. Thöle, S. S. Tsirkin, M. Wierzbowska, N. Marzari, D. Vanderbilt, I. Souza, A. A. Mostofi, J. R. Yates, *Journal of Physics: Condensed Matter* 32 (2020) 165902. doi:10.1088/1361-648x/ab51ff.
- [46] Q. Wu, S. Zhang, H.-F. Song, M. Troyer, A. A. Soluyanov, *Computer Physics Communications* 224 (2018) 405–416. doi:https://doi.org/10.1016/j.cpc.2017.09.033.
- [47] I. Galanakis, P. H. Dederichs, N. Papanikolaou, *Phys. Rev. B* 66 (2002) 174429. doi:10.1103/PhysRevB.66.174429.
- [48] G. Chang, S.-Y. Xu, H. Zheng, B. Singh, C.-H. Hsu, G. Bian, N. Alidoust, I. Belopolski, D. S. Sanchez, S. Zhang, et al., *Scientific reports* 6 (2016) 1–9. doi:https://doi.org/10.1038/srep38839.
- [49] L. Ding, J. Koo, L. Xu, X. Li, X. Lu, L. Zhao, Q. Wang, Q. Yin, H. Lei, B. Yan, Z. Zhu, K. Behnia, *Phys. Rev. X* 9 (2019) 041061. doi:10.1103/PhysRevX.9.041061.
- [50] A. Sakai, Y. P. Mizuta, A. A. Nugroho, R. Sihombing, T. Koretsune, M.-T. Suzuki, N. Takemori, R. Ishii, D. Nishio-Hamane, R. Arita, et al., *Nature Physics* 14 (2018) 1119–1124. doi:https://doi.org/10.1038/s41567-018-0225-6.
- [51] H. Reichlova, R. Schlitz, S. Beckert, P. Swekis, A. Markou, Y.-C. Chen, D. Kriegner, S. Fabretti, G. Hyeon Park, A. Niemann, S. Sudheendra, A. Thomas, K. Nielsch, C. Felser, S. T. B. Goennenwein, *Applied Physics Letters* 113 (2018) 212405. doi:10.1063/1.5048690.
- [52] J. Hu, B. Ernst, S. Tu, M. Kuveždić, A. Hamzić, E. Tafra, M. Basletić, Y. Zhang, A. Markou, C. Felser, A. Fert, W. Zhao, J.-P. Ansermet, H. Yu,

Phys. Rev. Applied 10 (2018) 044037. doi:10.1103/PhysRevApplied.10.044037.

- [53] Y. Yao, L. Kleinman, A. H. MacDonald, J. Sinova, T. Jungwirth, D.-s. Wang, E. Wang, Q. Niu, Phys. Rev. Lett. 92 (2004) 037204. doi:10.1103/PhysRevLett.92.037204.
- [54] A. Liechtenstein, M. Katsnelson, V. Antropov, V. Gubanov, Journal of Magnetism and Magnetic Materials 67 (1987) 65–74. doi:https://doi.org/10.1016/0304-8853(87)90721-9.
- [55] P. W. Anderson, Vol. 14 of Solid State Physics, 1963, pp. 99–214. doi:https://doi.org/10.1016/S0081-1947(08)60260-X.
- [56] M. Born, The Journal of Chemical Physics 7 (1939) 591–603. doi:10.1063/1.1750497.
- [57] R. Hill, Proceedings of the Physical Society. Section A 65 349–354. doi:10.1088/0370-1298/65/5/307.
- [58] V. Kanchana, G. Vaitheeswaran, A. Svane, Journal of Alloys and Compounds 455 (2008) 480–484. doi:https://doi.org/10.1016/j.jallcom.2007.01.163.
- [59] V. Kanchana, G. Vaitheeswaran, Y. Ma, Y. Xie, A. Svane, O. Eriksson, Phys. Rev. B 80 (2009) 125108. doi:10.1103/PhysRevB.80.125108.
- [60] V. Kanchana, EPL (Europhysics Letters) 87 (2009) 26006. doi:10.1209/0295-5075/87/26006.